Geomechanics and Engineering, *Vol. 34, No. 4 (2023) 449-459*
https://doi.org/10.12989/gae.2023.34.4.449

Physio-mechanical and X-ray CT characterization of bentonite as sealing material in geological radioactive waste disposal

Melvin B. Diaz[1a], Sang Seob Kim[1b], Gyung Won Lee[1c], Kwang Yeom Kim*[1], Changsoo Lee[2d], Jin-Seop Kim[2e] and Minseop Kim[2f]

[1]Department of Energy and Resources Engineering, Korea Maritime and Ocean University, 727, Taejongro, Yeongdo-gu, Busan, 49112, Republic of Korea
[2]Radioactive Waste Disposal Research Division, Korea Atomic Energy Research Institute, 111 Daedeok-dero 989 Beon-gil, Yuseong-gu, 34057, Republic of Korea

(*Received October 13, 2022, Revised July 18, 2023, Accepted July 19, 2023*)

Abstract. The design and development of underground nuclear waste repositories should cover the performance evaluation of the different components such as the construction materials because the long term stability will depend on their response to the surrounding conditions. In South Korea, Gyeonju bentonite has been proposed as a candidate to be used as buffer and backfilling material, especially in the form of blocks to speed up the construction process. In this study, various cylindrical samples were prepared with different dry density and water content, and their physical and mechanical properties were analyzed and correlated with X-ray CT observations. The main objective was to characterize the samples and establish correlations for non-destructive estimation of physical and mechanical properties through the utilization of X-ray CT images. The results showed that the Uniaxial Compression Strength and the P-wave velocity have an increasing relationship with the dry density. Also, a higher water content increased the values of the measure parameters, especially for the P-wave velocity. The X-ray CT analysis indicated a clear relation between the mean CT value and the dry density, Uniaxial Compression Strength, and P-wave velocity. The effect of the higher water content was also captured by the mean CT value. Also, the relationship between the mean CT value and the dry density was used to plot CT dry densities using CT images only. Moreover, the histograms also provided information about the samples heterogeneity through the histograms' full width at half maximum values. Finally, the particle size and heterogeneity were also analyzed using the Madogram function. This function identified small particles in uniform samples and large particles in some samples as a result of poor mixing during preparation. Also, the μ_{max} value correlated with the heterogeneity, and higher values represented samples with larger ranges of CT values or particle densities. These image-based tools have been shown to be useful on the non-destructive characterization of bentonite samples, and the establishment of correlations to obtain physical and mechanical parameters solely from CT images.

Keywords: bentonite; buffer material; dry density; EBS; X-ray

1. Introduction

Engineered Barrier Systems (EBS) are key elements of deep geological disposal of high-level radioactive waste (Ewing *et al*. 2016). EBS are composed of multiple disposal tunnels, from which smaller wells are drilled to allocate the spent fuel in canisters. Other components of EBS, are the buffer, and backfill materials (Yoon *et al.* 2021). The buffer material serves to cover the interior of the wells and isolate the canister from the host rock. Finally, once all the wells of a disposal tunnel are full, the tunnel is sealed with the backfill material. Since the early development of the concept of EBS, it was recognized that the properties of the host rock strongly affect its performance, and therefore a careful selection of the site should be carried out (Corkhill and Hyatt 2018, Villar *et al.* 2018, Wang *et al.* 2018, Rutqvist 2020). Moreover, the buffer material is meant to protect the canister from the deformation of the surrounding rock and isolate it physically, chemically, hydraulically, and biologically to block the outflow of radionuclides. On the other hand, the backfill is placed to hydraulically isolate the well, maintaining the cushioning material intact, and mechanically stabilize the shaft's entrance.

Various studies have assessed the performance of bentonite or mixtures of bentonite and sand to be used as buffer and backfill materials (Xu *et al.* 2016, Nasir *et al.* 2017, Liu *et al.* 2021, Chen *et al.* 2022).

Bentonite is mainly composed of clay minerals, and their properties are important as they influence the overall bentonite performance. Factors affecting the long-term performance of bentonite as cushioning materials include; swelling reduction, deterioration of sorption performance, formation of fast flow paths, and increase of hydraulic conductivity (Zeng *et al.* 2021). The long-term performance

*Corresponding author, Professor
E-mail: kykim@kmou.ac.kr
[a]Ph.D.
[b]Master student
[c]Master student
[d]Ph.D.
[e]Ph.D.
[f]Ph.D.

ISSN: 2005-307X (Print), 2092-6219 (Online)

evaluation should assess the potential changes in the properties such as the dry density, swelling characteristics, and others over time. In particular, different swelling pressures may arise during operation due to differences in material properties or ground water properties (Chen *et al.* 2019). Another long-term effect to be considered is the thermal gradient induced by the decay of the spent fuel in the canister (Villar *et al.* 2020), making this a thermal-hydrological-mechanical-chemical assessment of the evolution of bentonite properties.

Lee *et al*. (2019) experimentally analyzed the thermo-hydraulic-mechanical characteristics of Gyeongju bentonite buffer for high-level waste disposal facilities in Korea. They reported results on the uniaxial compressive strength (UCS), elastic modulus, Poisson's ratio, shear strength, and compaction characteristics, which are important parameters to guarantee the mechanical integrity of the engineered barrier. Furthermore, the thermal properties of this bentonite allow a rapid heat dissipation generated from the disposed waste to the surrounding rock, so that the temperature of the disposal container and buffer material do not exceed the set critical temperature. Moreover, they pointed out that the swelling pressure can serve as a sealing measure because it represents the pressure exerted on the outer wall as a result of the hydration reaction of bentonite in contact with groundwater in a limited space. Then, the proper characterization of the buffer and sealing materials is an important step during project design.

South Korea is working on the design and development of radioactive waste repositories, and testing the performance of local materials. Most domestic studies in Korea have been carried out with Ca bentonite made in Gyeongju by Cliriant Korea, which has produced mainly two types named KJ-I and KJ-II fabricated before and after 2015 respectively (Yoon *et al.* 2018). The thermal conductivity of KJ-II has been said to be higher due to a higher concentration of high thermal conductivity minerals such as Quartz, Cristobalite, and Calcite. Similarly, Yoo *et al.* (2016) evaluated the physical and chemical properties of KJ-II bentonite, and reported a water content of 10.96% and a moisture content of 12.31%. These values are in line with the requirements for the average water content of ≤13% with a max. of 15%, set for Ca bentonite as a buffer material (Kiviranta *et al.* 2011). On the other hand, the swelling index of KJ-II bentonite was 6.5 ml/2g, a value lower than the minimum of 10 ml/2g suggested by Kiviranta *et al*. (2011). Moreover, for cushioning materials to function properly as barriers, they must have a high swelling capacity. However, the swelling pressure must be maintained properly so as not to impose an excessive load on the canister and surrounding rock. In this regard, various studies have reported that heating induces volume contraction under loading (Kale *et al.* 2018, Wang *et al.* 2021). Park *et al*. (2021) studied the unsaturated and saturate behavior of Gyeongju bentonite under thermal effects and found volumetric contraction with temperature as well as irreversible permeability changes, where hydraulic conductivity increased with increasing temperature. The results showed how after initial disposition, the water suction pressure increased rapidly with increasing temperature. However, when the water content was kept constant, the suction pressure remained nearly constant with a slight decrease with increasing temperature. All these examples show how the complex thermal-hydrological-mechanical-chemical conditions in which the engineered barrier is placed, induce constant changes in its physical and mechanical properties.

Recently, the usage of pre-fabricated bentonite blocks was proposed to speed up the construction process (Tan *et al.* 2021). Since South Korea is also considering this alternative construction method, in this work we evaluated the basic physio-mechanical properties of Gyeongju bentonite under the assumption that the buffer material will be pre-fabricated and installed in the form of blocks. The samples were fabricated with varying water content and dry density. Moreover, X-ray CT technology was used to internally inspect the samples. The main objective was to characterize the samples and establish correlations for non-destructive estimation of physical and mechanical properties such as the dry density and UCS through the utilization of X-ray CT images. The detailed sample preparation process and results are as follows.

2. Materials and methods

2.1 Cylindrical samples of Gyeongju bentonite

The laboratory experiments presented here were carried out with Gyeongju bentonite, which has been proposed as buffer material for High-level Radioactive Waste repositories in Korea. As a buffer material, bentonite blocks generally need to have a dry density of 1.6 g/cm^3 or more to secure their stability as an engineered barrier material (Lee *et al.* 2010). In this work, cylindrical samples were manufactured with different dry densities (1.4, 1.6, and 1.8 g/cm^3), and water content (10%, 20%, and 30%) using Gyeongju bentonite powder. The sample preparation process is shown in Fig. 1. First, the amount of dried bentonite powder (Fig. 1(a)) and water were determined according to the predefined water content, along with the volume capacity of the compression cell. Then, the combination was mixed evenly using a stirrer (Fig. 1(c)). Finally, the mixture was placed into the compression cell, and loaded until the desired dry density was reached. The samples have a final dimension of 3.0 cm in diameter and 5.0 cm in height. When the dry density was set to 1.4 g/cm^3, it was possible to manufacture all cases of 10%, 20%, and 30% of water content. However, when the dry density was 1.6 g/cm^3, only samples of 10% and 20% were manufactured. Similarly, when the dry density was 1.8 g/cm^3 only samples of 10% of water content were made. This is because it was impossible to increase the maximum load of the compression system beyond the allowable strength of the cell for sample preparation. Then, due to this limitation, three sets of six types of samples were prepared with dry density and water content characteristics mentioned above. The first two sets were used for UCS and P-wave wave velocity testing, and the third for X-ray CT analysis.

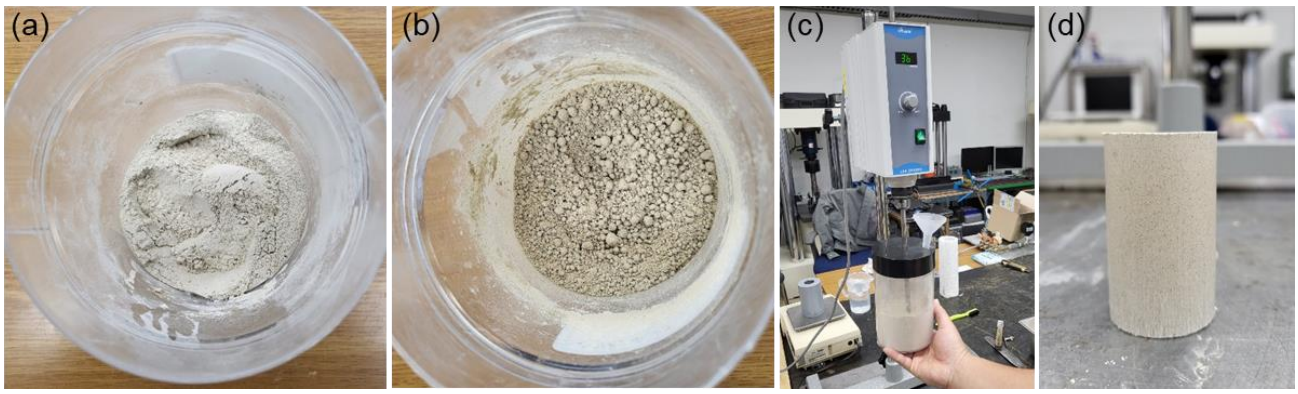

Fig. 1 Process of sample preparation. Gyeongju bentonite in its powder form (a). Water is added at a specified proportion (b). Then, the combination is mixed mechanically (c). Finally, the mixture is placed into a mold and loaded until the desired dimensions and density are reached (d)

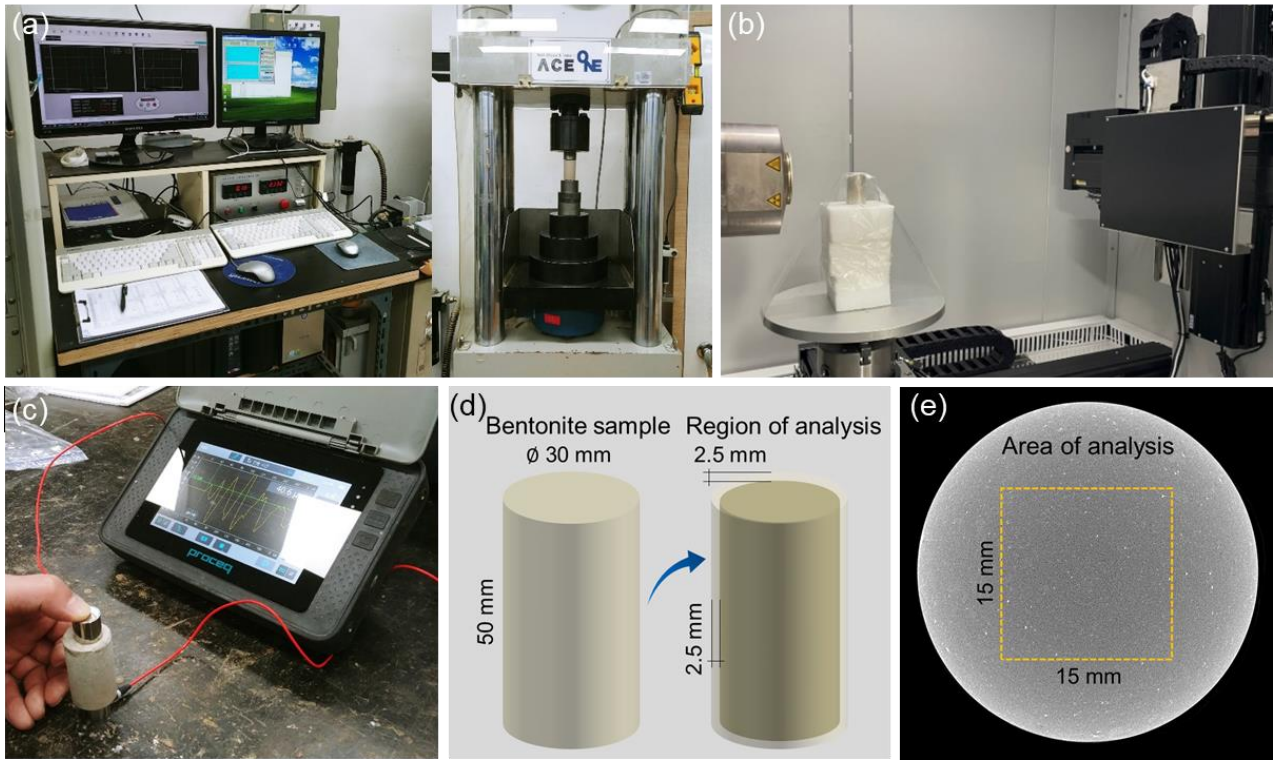

Fig. 2 Testing equipment. Uniaxial compressive strength apparatus (a). X-ray CT equipment at KMOU (b). Equipment for elastic wave velocity measurement (c). Schematic of the final dimensions of the bentonite sample as well as the selected region of analysis for X-ray CT evaluation (d). X-ray CT cross section of bentonite sample indicating the area for homogeneity and particle size analysis (e)

2.2 UCS, P-wave velocity and X-ray equipment

The first two sets of samples were used to perform UCS and P-wave velocity tests. UCS tests were carried out using the ACEONE 08274628 compression test equipment, which has a maximum load capacity of 196.1 kN(20 ton-force) (Fig. 2(a)). The tests were conducted following the ASTM D7012-14e1, under displacement control. All stresses during testing were automatically recorded through a data logger for later analysis.

The elastic wave (P-wave) velocity was measured using an ultrasonic speed tester (Proceq's Pundit PL-2), The resonant frequency of the transmitter and receiver was 70 kHz (Fig. 2(c)). The range of seismic wave velocity was about 700~1300 m/s. Finally, only the third set of samples was taken for X-ray CT inspection. The X-ray CT equipment used in this study is the TVX-IMT225CT equipment of Tech Valley Co., Ltd., which includes a tube with a voltage of up to 225 kV and a tube current of 200 μA, and a 500 mm × 500 mm flat-panel detector (Pixel size 100 μm) (Fig. 2(b)). The sample is placed on a rotating pedestal, and subjected to X-rays. As the X-rays penetrate the material, some are absorbed while others go through,

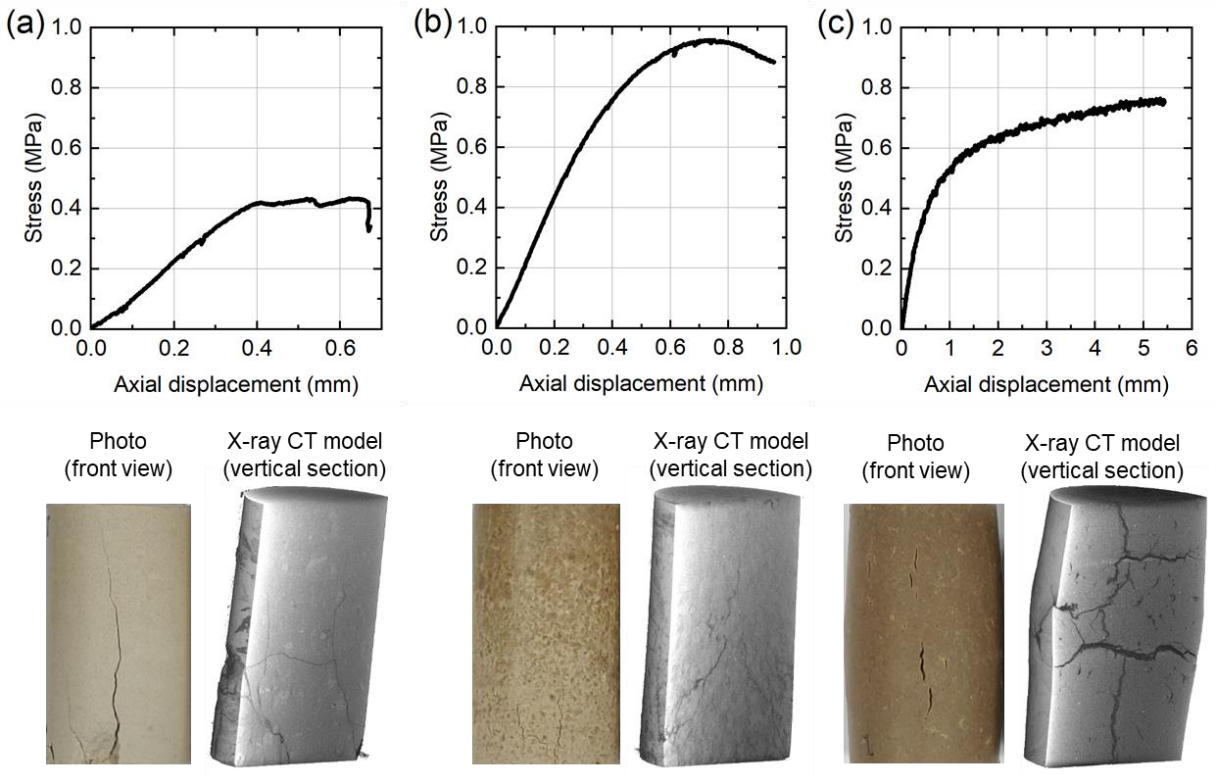

Fig. 3 Fracture behavior of bentonite samples under uniaxial compression. Axial stress against axial displacement for samples of equal dry density (1.4 g/cm^3) but different water content; 10% (a), 20% (b), and 30% (c). Photographs and X-ray CT models of the samples are added to support the analysis. As the water content increases, there is a transition from a brittle to a ductile failure

although they are attenuated. The number of X-rays that are able to pass the material is registered at the detector and serves to reconstruct the image based on the CT values. In this analysis, the CT scanning conditions were determined through an image optimization process. The final scanning conditions were 90 kV tube voltage, 135 μA tube current, 3 fps exposure time, 2900 total projections, and 17 minutes total recording time. The spatial resolution of the image was taken at 55 μm based on the pixel pitch. After reconstruction, a smaller inner region was used for analysis (Fig. 2(d)). Finally, the insert in Fig. 2(e) shows a typical X-ray CT cross section indicating the area for homogeneity and particle size analysis. The square region of 15×15 mm was taken at the center of the cross section and the sample's mid-height.

2.3 Madogram function

The degree of homogeneity inside the bentonite samples was analyzed by applying the Madogram function to X-ray CT images. This quantitative characterization method of the stochastic spatial distribution of material constituents is called the two-point correlation. The two-point correlation technique was applied to materials composed of two or more phases when typical binarization methods did not allow the separation of the internal structures of a material composed of two or more phases (Ha *et al*. 2020). Then, the Madogram function was applied to X-ray CT images, and the average particle size as well as the distribution of the components were determined. The function was implemented through a Python-based in-house code written for this purpose. The calculation process is as follows. For a given CT image, two random points separated by a pre-defined length (in pixels) are randomly generated. Then, the CT image pixel values at these points and the length separating them are used to calculate the arithmetic mean according to Eq. (1).

$$\mu_i^{\Delta P} = \frac{\sum_{j=1..N} \left| P1_{L_{i,j}} - P2_{L_{i,j}} \right|}{N} \quad (1)$$

where P1 and P2 represent the two randomly generated points, and L is the pre-defined length. The calculation was gradually increased from the L value of 0, and up to half the size of the image domain. Typically, the μ value increases with increasing L size. However, at a certain L size, the μ value peaks and later decreases. This maximum represents the mean size of the particles present in the image, and the value at this time is called μ_{max}.

3. Results and discussion

3.1 UCS and P-wave velocity

Results of the UCS and P-wave velocity tests for the first two sets of bentonite samples are presented in Table 1.

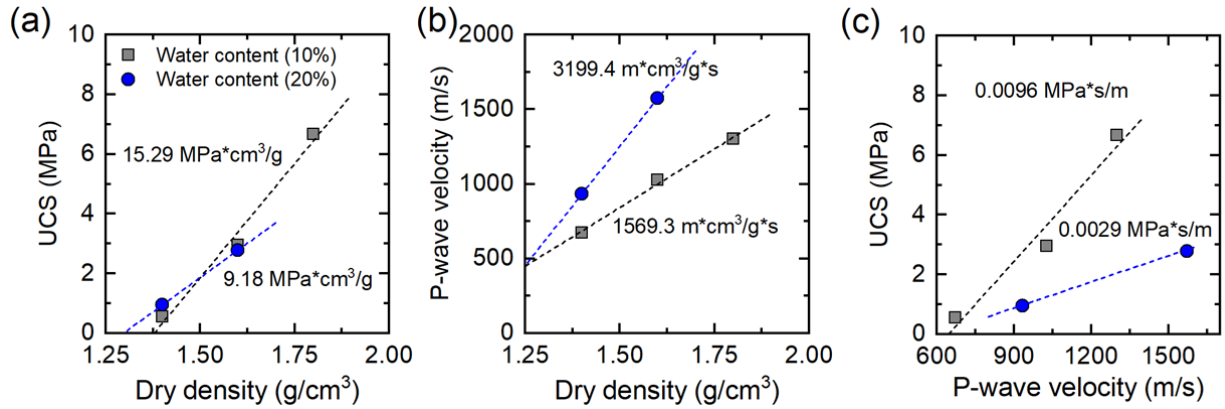

Fig. 4 Results of uniaxial compressive strength (a) and P-wave velocity (b) against dry density for the two sets of samples with 10% and 20% of water content. UCS versus P-wave velocity (c)

Table 1 Physical and mechanical properties of bentonite samples

No.	ID	Water content (%)	Wet density (g/cm^3)	UCS (MPa)	P-wave velocity (m/s)
1	1.4 (10%) -1	10	1.489	0.434	706
2	1.4 (10%) -2	10	1.479	0.675	636
3	1.4 (20%) -1	20	1.661	0.956	939
4	1.4 (20%) -2	20	1.648	0.939	927
5	1.4 (30%) -1	30	1.798	0.766	1586
6	1.4 (30%) -2	30	1.810	0.859	1555
7	1.6 (10%) -1	10	1.692	2.738	1030
8	1.6 (10%) -2	10	1.708	3.156	1022
9	1.6 (20%) -1	20	1.889	2.833	1578
10	1.6 (20%) -2	20	1.888	2.733	1568
11	1.8 (10%) -1	10	1.887	5.894	1271
12	1.8 (10%) -2	10	1.904	7.445	1327

The range of measured values shows very small strength values from 0.4 to 7.4 MPa. Moreover, there was no significant difference in uniaxial compressive strength between samples with the same dry density but different water content. However, the deformation behavior before failure showed a difference depending on the water content (Fig. 3). Samples with low water content described a typical brittle fracture behavior. However, as the water content increased, high strain occurred before failure and a more ductile behavior was observed after failure. This transition is due to Gyeongju bentonite's optimum water content of 15.7% given by Kim et al. (2018). This means that the case of 30% of water content falls on the wet side of the compaction curve where the excess of pore pressure decreases the soil shear strength.

Fig. 4 shows relationships among dry density, UCS, and P-wave velocity. The results of UCS and P-wave velocity tests shown here are the averages of each pair of samples under the same sample type (dry density and water content, Table 1). The UCS value increased with increasing dry density (Fig. 4(a)), and although the effect of the water content was small, it showed a smaller gradient for cases with a higher water content of 20%. Similarly, the P-wave velocity also increased with increasing dry density. However, the effect of the water content was more evident and opposite to that observed for the UCS, with larger P-wave velocities for samples with the same dry density but higher water content (Fig. 4(b)). This resulted in a larger gradient for samples with a higher water content of 20%. The P-wave velocity is affected by the individual characteristics of the constituting material. As the voids in samples decrease, especially in those with higher dry density, the elastic wave velocity increases. Lastly, the uniaxial compressive strength and the P-wave velocity also showed a linearly increasing relationship, with a smaller gradient for cases with a higher water content (Fig. 4(c)).

3.2 Physical and mechanical properties derived from X-ray CT images

The internal structure of bentonite samples was evaluated through X-ray CT scanning using the third set. Because the bentonite samples are composed of a mixture of bentonite powder and water, dry density variations can occur due to localized changes. Fig. 5 shows the histograms as well as the full width at half maximum of all samples. When the water content remained the same, the mean CT (μ) value increased for increasing dry density. This behavior was the same for samples with 10% and 20% of water content (Figs. 5(a) and 5(b)). In other words, the dry density is proportional to the mean CT value. On the other hand, the mean CT value did not always increase with increasing water content for samples of the same dry density. For example, cases of 1.4 g/cm^3 of dry density showed an increasing trend for the water content of 10% and 20%. However, with a further increase in the water content, the mean CT value decreased again. As explained before, the transition in the UCS values for samples under the same dry density, but increasing water content is due to the optimum water content, which indicated that only the first case of 10% of water content fell on the dry side of the compaction curve. This difference can also be observed in the histograms. Fig. 5(c) compares the cases of 10% and 30% of water content. Although their mean values are similar, their frequencies are different, with a higher value for the

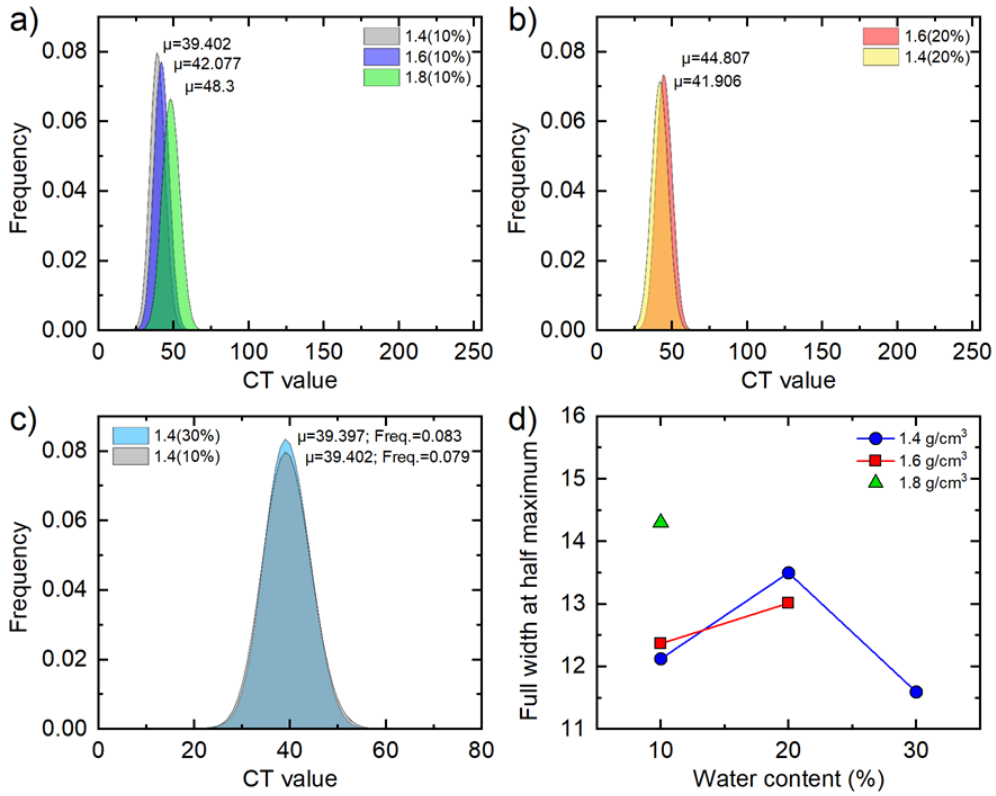

Fig. 5 Histograms and full width at half maximum of X-ray CT images. The histograms and their mean values (μ) correspond to the volume or region of interest of the bentonite samples shown in Fig. 1. Bentonite samples with 10% of water content (a), 20% of water content (b), and a comparison of samples of 1.4 g/cm^3 but 10% and 30% of water content (c). Last, the histogram's full width at half maximum for all samples (d)

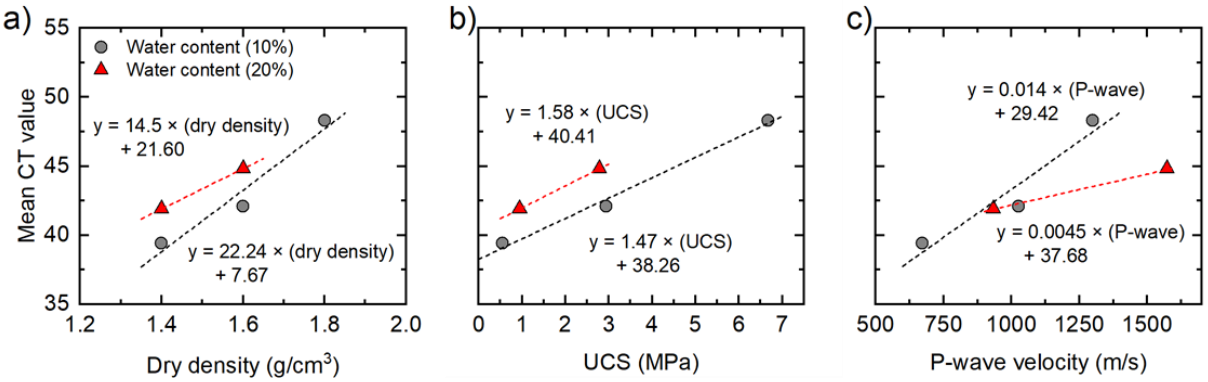

Fig. 6 Results of mean CT values against the dry density (a), uniaxial compressive strength (b), and P-wave velocity (c). The mean CT values are the average of the voxels contained in the region of analysis (Fig. 2(d))

case of 30% of water content. This higher frequency implies that the sample has a higher homogeneity because the CT values under the curve are closer to the mean. To quantify this, we employed the histograms' full width at half maximum. The results are shown in Fig. 5(d), where the full width at half maximum increases with increasing water content. However, with further increase of water content, the value tended to fall. Our interpretation of this increase on the full width is that, as the water content increases, some regions absorb more water, become denser, and create large particles, making the sample more heterogeneous. However, if further water is added, higher lubrication and mobilization of soil particles occur which results in a more homogeneous sample indicated by a lower full width at half maximum and a higher frequency. This is supported by the average particle estimation presented in the next section.

Pixels comprising an X-ray CT image have a direct relationship with the density of the material. Because of this, the correlation between the sample physio-mechanical properties and the mean CT values (of the region of analysis, Fig. 2(d)) were analyzed in Fig. 6. The mean CT value tends to increase with the bentonite dry density (Fig. 6(a)). Also, for samples with the same dry density, the mean CT values were higher when the water content was higher (20%). This is because, with higher water content, the samples were able to reach higher densities. However, the

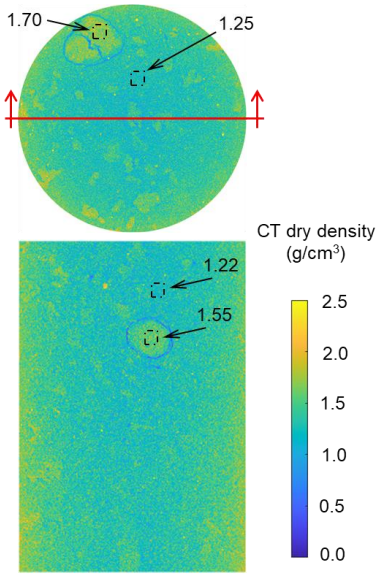

Fig. 7 Dry density based on CT values. The figure was plotted using the relation obtained for samples with 10% of water content (Fig. 6(a)). Red arrows indicate the cutting plane. The sample was prepared with a dry density of 1.4 g/cm^3 and a water content of 10%

gradient of this relationship showed a decrease from 22.2 to 14.5 when the water content increased from 10% to 20%. Nevertheless, this trend is not conclusive due to the low number of samples used here, and therefore further characterization with a larger number of samples is desirable. Similarly, the correlation between the mean CT and the UCS also shows a positive linear relationship (Fig. 6(b)). Again, the mean CT values were higher for cases with higher water content (20%), and their gradients were similar, with 1.47 and 1.58 for samples of 10% and 20% of water content, respectively. Finally, Fig. 6(c) shows the relationship between the mean CT value and the P-wave velocity. Like the other relations, the mean CT value increased with increasing P-wave velocity. However, the gradient decreased from 0.014 to 0.0045 as the water content increased from 10% to 20%. This shows how the mean CT value became more constant regardless of the P-wave velocity, presumably due to a better homogenization of the mixture at higher water contents.

Despite the small number of tested samples, these relationships between physio-mechanical properties and the mean CT values are useful non-destructive tools to inspect and obtain direct values of the properties using CT images only. For example, the case of bentonite samples subjected to hydration or temperature, the internal changes can be quantified using these relationships. Likewise, for long tests, periodic CT scans will offer an opportunity to track and follow changes in physical and mechanical properties.

These will be addressed in future works. As shown above, the CT images captured the changes induced by the different dry densities and water contents. Then, we used the relationship between the dry density and the mean CT value as a reference to derive local density variations from the CT images. Fig. 7 shows a cross and a vertical section of a sample with values of the so-called CT dry density. Red arrows indicate the location of the cutting plane from where the vertical section was obtained and small black-squares show areas selected for comparison. Although this sample has a dry density of 1.4 g/cm^3, and water content of 10%, the selected areas indicate local variations in dry density within the samples. For example, in the cross section, the area inside a large grain has a higher density than the samples' designed dry density of 1.4 g/cm^3. In contrast, the area in the middle falls under this value. Moreover, this figure shows how the area surrounding the large grains has a low density. These void areas may have resulted from drying since, after preparation, the samples were exposed to ambient conditions. In summary, this approach facilitates the non-destructive characterization of local changes in physio-mechanical properties using CT images only for sets of samples with equal water content.

3.3 Measurement of particle size and homogeneity based on X-ray CT images

The particle size and homogeneity were analyzed using the areas of analysis shown in Fig. 8. These images were taken from cross sections at mid-height of the samples as explained in Fig. 2(e). Table 2 shows the results of L and μ_{max} from the Madogram function applied to the six samples of set 3 (Fig. 8). Since all samples were made of bentonite powder, similar values can be expected. However, only the values of samples 3 to 6 kept certain similarities, while those of samples 1 and 2 presented larger values. This difference can even be observed with the naked eye from the X-ray CT images of bentonite samples shown in Fig. 8, where Figs. 8(a) and 8(b) have large particles, while Figs. 8(c)-(f) are uniform. Then, the L values for samples 1 and 2 (Figs. 8(a)-(b)) are thought to have resulted from the bentonite sample preparation process. Low water content, along with poor mixing during the preparation of these samples generated relatively large particles that resulted in larger values of L. Larger particles can also be observed from Fig. 7, where those particles display higher CT dry densities than the media.

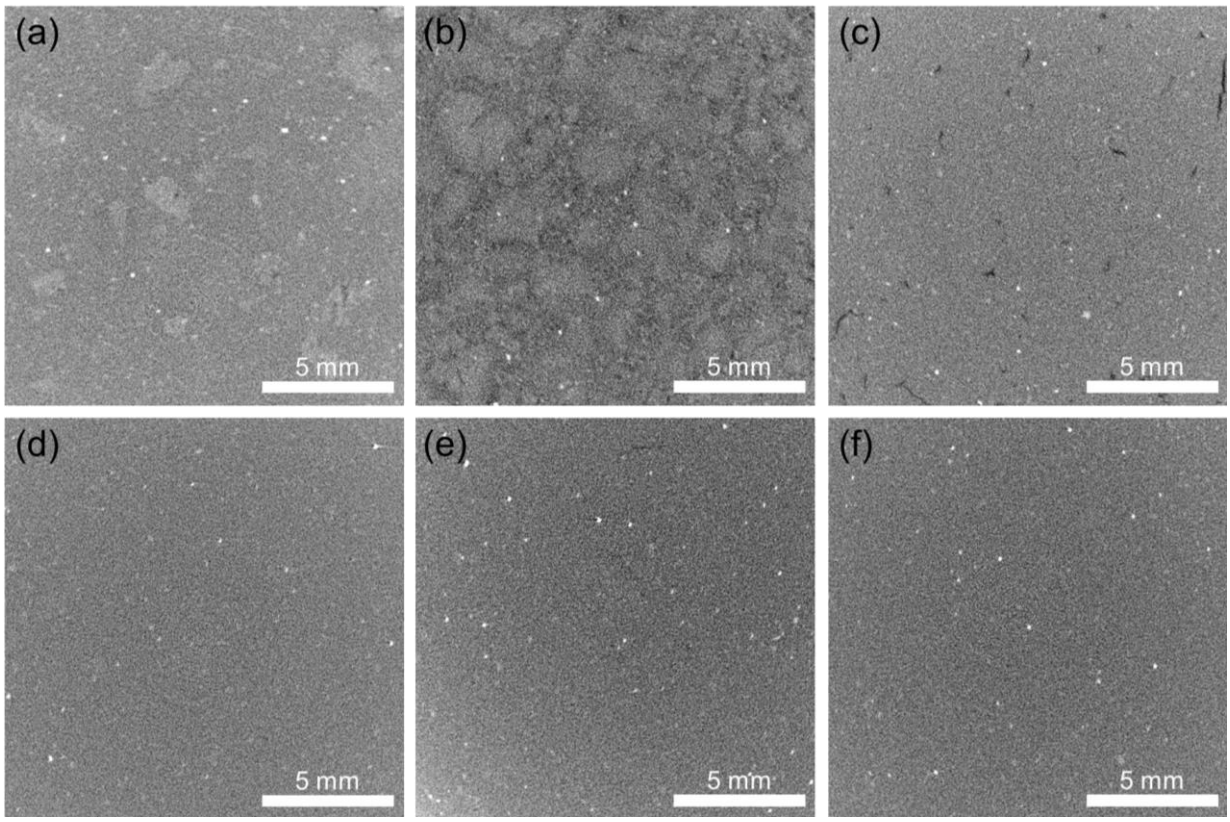

Fig. 8 X-ray CT images used for homogeneity and particle size analyses. The areas were taken from cross sections at half the sample height as indicated in Fig. 2(e). The images correspond to samples prepared with dry density (g/cm^3) and water content (%) of: 1.4(10%) (a), 1.4(20%) (b), 1.4(30%) (c), 1.6(10%) (d), 1.6(20%) (e), and 1.8(10%) (f)

Table 2 Results of the Madogram function

No.	Dry density (g/cm^3)	Water content (%)	L (pixels) [domain size: 902]	μ_{max}
1	1.4	10%	25	22.56
2	1.4	20%	56	32.44
3	1.4	30%	9	27.99
4	1.6	10%	6	25.60
5	1.6	20%	4	30.06
6	1.8	10%	4	29.30

On the other hand, the L values from Table 2 for samples with a dry density of 1.4 g/cm^3 are in line with the heterogeneity assessment presented in the previous section through the histograms full width at half maximum. Then, this explains why the case with 20% of water content reported a higher heterogeneity.

Moreover, the applicability of the Madogram function to X-ray CT images was also confirmed by plotting the standard deviation of CT values per image against μ_{max} in Fig. 9(a). The results indicate a linear relationship between these two parameters, with a coefficient of determination (r^2) of 0.91. Next, the typical evolution of the $\mu r\Delta P$ value from the X-ray CT images of the bentonite samples is shown in Fig. 9(b). Here, three samples of dry density (g/cm^3) and water content (%) of 1.6(10%), 1.6(20%), and 1.8(10%) were selected, and they correspond to the CT cross sections shown in Figs. 8(d)-8(f) respectively. The $\mu^{\Delta P}{}_L$ values depicted an increasing trend. Therefore, μ_{max} was taken as the inflection point where the curve transitions from the initial linear region to the later stage with a stable but low incremental rate. As reported in Table 2, the L distances for these cases are not only small but similar, and are in line with the results expected for these samples composed of bentonite powder. However, the μ_{max} values showed a certain difference. For example, the case with a dry density (g/cm^3) and water content (%) of 1.6(10%) reported a μ_{max} value of 25.6. On the other hand, μ_{max} was 30.06 and 29.3 for the other two samples with a dry density (g/cm^3) and water content (%) of 1.6(20%), and 1.8(10%) respectively.

The difference in μ_{max} values for the images presented in Fig. 9(b) can be explained in terms of the heterogeneity of the selected area, or in other words, the histograms' full width at half maximum. This is the same approach adopted in section 3.2 to compute the heterogeneity of the entire volume. However, here it is used to evaluate the heterogeneity of the cross sections presented in Figs. 8(d)-8(f). The histograms of those sections are shown in Fig. 10(a), with their mean CT value (μ) and full width at half maximum in brackets. The difference in μ_{max} values correlates with the full width at half maximum, where the first case with a dry density (g/cm^3) and a water content (10%) of 1.6(10%) reported a value of 54.3. In contrast, the other two cases with higher μ_{max} values also reported higher values of the full width at half maximum.

To observe the correlation between μ_{max} and the histogram's full width at half maximum, we plotted those

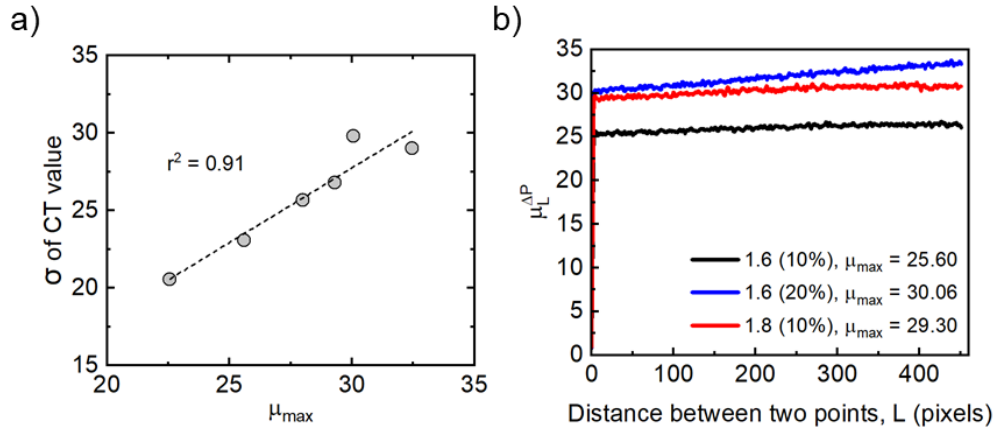

Fig. 9 Standard deviation (σ) of CT values versus μ_{max} for the six samples (a). Results from Madogram function showing μLΔP against the mean distance between two points (L) (b). These curves correspond to samples prepared with dry density (g/cm^3) and water content (%) of: 1.6(10%) [black], 1.6(20%) [blue], and 1.8(10%) [red]

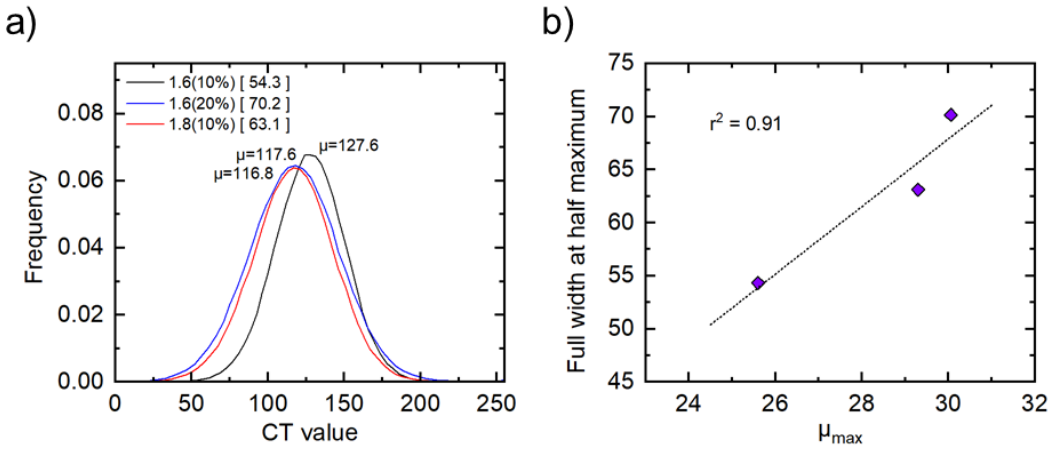

Fig. 10 (a) Histograms of CT values of the areas of analysis (Fig. 8(d)-(f)) of samples with dry density (g/cm^3) and water content (%) of: 1.6(10%), 1.6(20%), and 1.8(10%). The mean CT values (μ) and full width at half maximum (in brackets) are provided. (b) Full width at half maximum against μ_{max} showing a positive relation

parameters in Fig. 10(b). The results show a clear positive correlation between these two parameters. This means that μ_{max} also carries information about the composition of the images, or more precisely, about their heterogeneity. This characteristic of μ_{max} has been reported previously. Ha et al. (2020) carried out a study using images of different rocks that included Sandstone, Diorite, Gneiss, Anorthosite, and Amphibolite. The authors pointed out that μ_{max} can serve as an indication of the homogeneity of the rock image. Therefore, the results from the Madogram function indicate that although these three samples had similar particle sizes (L values), two of them were more heterogeneous.

The results presented in this study are important steps in the characterization and analysis of local soils that are candidates for buffer materials in EBS, and prepared in the form of prefabricated blocks. Firstly, multiple samples with dry densities of 1.4, 1.6, and 1.8 g/cm^3, and water content of 10%, 20%, and 30% were prepared using Gyeongju bentonite. Second, the X-ray CT technique was useful to establish correlations between the dry density, UCS and P-wave velocity and the CT values. The correlations allowed the estimation of these physio-mechanical properties directly from the CT images. For example, it was possible to quantify local dry density variations in samples, like those between the media and large particles in some samples. This advantage will be used in future works when the samples will be tested under thermal and hydration conditions. As the hydration front advances, this technique will serve to quantify the changes in the physio-mechanical properties without destroying the sample, and therefore securing the continuation of the test. These and other image-based tools will be incorporated into future studies.

4. Conclusions

An analysis of the physio-mechanical properties of cushioning materials as engineering barriers for underground nuclear waste repositories has been presented. Three sets of six cylindrical bentonite samples were prepared using Gyeongju bentonite with the assumption that they will be pre-fabricated and installed in the form of blocks. The samples were prepared with varied dry density and water content. Properties such as the Uniaxial

Compressive Strength (UCS) and the P-wave velocity were measured. Then, the samples were subjected to X-ray CT inspection for further characterization. The main objective was to characterize the samples and establish correlations for non-destructive estimation of physical and mechanical properties through the utilization of X-ray CT images. The conclusions are as follows.

The UCS and the P-wave velocity showed a linear and increasing relationship with the dry density. The water content played an important role and increased the P-wave velocity values for samples with the same dry density, but higher water content. Also, the P-wave velocity gradient was higher for samples with higher water content. Conversely, the effect of the water content on the UCS initially increased, but later reduced. This transition was associated to the optimum water content of Gyeongju bentonite.

X-ray CT technology aided the further characterization of the bentonite samples. The full width at half maximum of the histograms was used to estimate the heterogeneity, which showed an initial increasing trend under increasing water content for samples of equal dry density. However, with further water increase, the full width at half maximum decreased. At the same time, the Madogram function was also used to estimate the particle size and heterogeneity using CT cross sections. It was found that the particle size was similar for most cases, with exception of two that returned overestimated values, which was associated with the formation of large particles due to poor mixing of bentonite during sample preparation. Moreover, the sample heterogeneity was also captured by the μ_{max}, which showed a positive correlation with the full width at half maximum of the images' histograms.

On the other hand, the mean CT value increased with increasing dry density, UCS, and P-wave velocity. Also, the mean CT values were higher for samples with the same dry density and UCS, but higher water content. However, the gradients of mean CT value and dry density, as well as P-wave velocity decreased for samples with higher water content. Moreover, the correlations between the mean CT values and the dry densities were used to obtain dry densities from CT images and therefore quantify inner local variations such as larger particles with higher dry density than the media solely from CT images.

Despite the consideration of three different dry densities and three water contents for the examined samples, the available dataset remains insufficient to establish robust relationships between physio-mechanical properties and CT values. Therefore, it is recommended to incorporate samples with varying conditions to enhance these relations. Nevertheless, these image-based tools have been shown to be practical and convenient for the non-destructive characterization of samples and direct estimation of physical and mechanical properties such as the dry density using images only.

Acknowledgments

This work was supported by the Institute for Korea Spent Nuclear Fuel (iKSNF) and National Research Foundation of Korea (NRF) grant funded by the Korea government (Ministry of Science and ICT, MSIT)(No. 2021M2E1A1085197 & No. 2021R1A2C2011634).

References

Chen, Y.G., Liu, L.N., Ye, W.M., Cui, Y.J. and Wu, D.B. (2019), "Deterioration of swelling pressure of compacted Gaomiaozi bentonite induced by heat combined with hyperalkaline conditions", *Soils Found.*, **59**(6), 2254-2264. https://doi.org/10.1016/j.sandf.2019.12.008.

Chen, Y.G., Cai, Y.Q., Pan, K., Ye, W.M. and Wang, Q. (2022), "Influence of dry density and water salinity on the swelling pressure and hydraulic conductivity of compacted GMZ01 bentonite–sand mixtures", *Acta Geotechnica*, **17**(5), 1879-1896. https://doi.org/10.1007/s11440-021-01305-7.

Corkhill, C. and Hyatt, N. (2018), *Nuclear Waste Management*, IOP Publishing, Bristol, England.

Ewing, R.C., Whittleston, R.A. and Yardley, B.W., (2016), "Geological disposal of nuclear waste: a primer", *Elements*, **12**(4), 233-237. https://doi.org/10.2113/gselements.12.4.233.

Ha, S.J., Jeong, Y.J. and Yun, T.S., (2020), "Parameterization of the representative sizes of microstructural features in rocks using 3D X-ray computed tomographic images", *Comput. Geosci.*, **144**, 104590. https://doi.org/10.1016/j.cageo.2020.104590.

Kale, R.C. and Ravi, K. (2018), "Influence of thermal loading on index and physicochemical properties of Barmer bentonite", *Appl. Clay Sci.*, **165**, 22-39. https://doi.org/10.1016/j.clay.2018.07.039.

Kim, J.S., Yoon, S., Cho, W.J., Choi, Y.C. and Kim, G.Y. (2018), "A Study on the Manufacturing Characteristics and Field Applicability of Engineering-scale Bentonite Buffer Block in a High-level Nuclear Waste Repository", *Journal of Nuclear Fuel Cycle and Waste Technology*, **16**(1), pp.123-136. (In Korean). https://doi.org/10.7733/jnfcwt.2018.16.1.123.

Kiviranta, L. and Kumpulainen, S. (2011), "Quality control and characterization of bentonite materials", Research Reprot No. POSIVA-WR--11-84; Posiva Oy, Helsinki, Finland.

Lee, J.H., Lee, M.S., Choi, H.J. and Choi, J.W. (2010), "Temperature effect on the swelling pressure of a domestic compacted bentonite buffer", *J. Nuclear Fuel Cycle Waste Tech.*, **8**(3), 207-213. (In Korean). https://jnfcwt.or.kr/journal/viewPDF.php?key=escce64/Lcc=.

Lee, C., Yoon, S., Cho, W.J., Jo, Y., Lee, S., Jeon, S. and Kim, G.Y., (2019), "Study on thermal, hydraulic, and mechanical properties of KURT granite and Gyeongju bentonite", *Special issue on In-DEBS in KURT, J. of Nuclear Fuel Cycle and Waste Tech*, **17**, 65-80. (In Korean). https://doi.org/10.7733/jnfcwt.2019.17.S.65.

Liu, Z.R., Ye, W.M., Cui, Y.J., Zhu, H.H., Wang, Q. and Chen, Y.G., (2021), "Development of swelling pressure for pellet mixture and compacted block of GMZ bentonite", *Constr. Build. Mater.*, **301**, 124080. https://doi.org/10.1016/j.conbuildmat.2021.124080.

Nasir, O., Nguyen, T.S., Barnichon, J.D. and Millard, A. (2017), "Simulation of hydromechanical behaviour of bentonite seals for containment of radioactive wastes", *Can. Geotech. J.*, **54**(8), 1055-1070. https://doi.org/10.1139/cgj-2016-0102.

Park, S., Yoon, S., Kwon, S., Lee, M.S. and Kim, G.Y., (2021), "Temperature effect on the thermal and hydraulic conductivity of Korean bentonite buffer material", *Progress Nuclear Energy*, **137**, 103759. https://doi.org/10.1016/j.pnucene.2021.103759.

Rutqvist, J. (2020), "Thermal management associated with

geologic disposal of large spent nuclear fuel canisters in tunnels with thermally engineered backfill", *Tunn. Undergr Sp. Tech.*, **102**, 103454. https://doi.org/10.1016/j.tust.2020.103454.

Tan, Y., Zhang, H., Zhang, T., Zhang, G., He, D. and Ding, Z. (2021), "Anisotropic hydro-mechanical behavior of full-scale compacted bentonite-sand blocks", *Eng. Geol.*, **287**, 106093. https://doi.org/10.1016/j.enggeo.2021.106093.

Villar, M.V., Iglesias, R.J., Gutiérrez-Álvarez, C. and Carbonell, B., (2018), "Hydraulic and mechanical properties of compacted bentonite after 18 years in barrier conditions", *Appl. Clay Sci.*, **160**, 49-57. https://doi.org/10.1016/j.clay.2017.12.045.

Villar, M.V., Iglesias, R.J., García-Siñeriz, J.L., Lloret, A. and Huertas, F. (2020), "Physical evolution of a bentonite buffer during 18 years of heating and hydration", *Eng. Geol.*, **264**, 105408. https://doi.org/10.1016/j.enggeo.2019.105408.

Wang, J., Chen, L., Su, R. and Zhao, X. (2018), "The Beishan underground research laboratory for geological disposal of high-level radioactive waste in China: planning, site selection, site characterization and in situ tests", *J. Rock Mech. Geotech. Eng.*, **10**(3), 411-435. https://doi.org/10.1016/j.jrmge.2018.03.002.

Wang, Q., Su, W., Ye, W., Zhang, Y. and Chen, Y. (2021), "Analysing the volume change behaviour of compacted bentonites upon THM processes based on the framework of BExM model", *Environ. Earth Sci.*, **80**(18), 1-12. https://doi.org/10.1007/s12665-021-09885-z.

Xu, L., Ye, W.M., Chen, B., Chen, Y.G. and Cui, Y.J. (2016), "Experimental investigations on thermo-hydro-mechanical properties of compacted GMZ01 bentonite-sand mixture using as buffer materials", *Eng. Geol.*, **213**, 46-54. https://doi.org/10.1016/j.enggeo.2016.08.015.

Yoo, M., Choi, H.J., Lee, M.S. and Lee, S.Y. (2016), "Measurement of properties of domestic bentonite for a buffer of an HLW repository", *J. Nuclear Fuel Cycle Waste Tech.*, **14**(2), 135-147. (In Korean). https://doi.org/10.7733/jnfcwt.2016.14.2.135.

Yoon, S., Cho, W., Lee, C. and Kim, G. (2018), "Thermal conductivity investigation of Korean bentonite buffer materials", *Proceedings of the Korean Radioactive Waste Society Conference*, Busan, Republic of Korea, May.

Yoon, S., Kim, M.S., Kim, G.Y. and Lee, S.R., (2021), "Contemplation of relative hydraulic conductivity for compacted bentonite in a high-level radioactive waste repository", *Annal. Nuclear Energy*, **161**, 108439. https://doi.org/10.1016/j.anucene.2021.108439.

Zeng, Z., Cui, Y.J. and Talandier, J., (2021), "Long-term effect of water chemistry on the swelling pressure and hydraulic conductivity of compacted claystone/bentonite mixture with technological gaps", *Eng. Geol.*, **295**, 106432. https://doi.org/10.1016/j.enggeo.2021.106432.

IC